Uncovering crystal growth and regeneration mechanism to control crystal morphology: the case study of aceclofenac

Longping Jiang[1], Wenqian Chen[2], Limin Zhou[1], Li Xu[1], Feiqiang He[1], Jerry Y Y Heng[3], Hamza Shehzad[1], Jinbo Ouyang[1,*]

[1]School of Chemistry and Materials Science, East China University of Technology, Nanchang 330013, China

[2]Department of Pharmacy, National University of Singapore, 117544, Singapore

[3]Department of Chemical Engineering, Imperial College London, South Kensington Campus, London SW7 2AZ, UK

[*]Corresponding author: Jinbo Ouyang, oyjb1001@163.com

Abstract: The study of crystal growth and regeneration mechanisms is of great significance for controlling the morphology of crystals. Through the investigation of the recovery and regrowth processes of crystals, we have revealed the regeneration mechanism of aceclofenac (ACF) crystals and the influence of hydroxypropyl methylcellulose (HPMC) on the regeneration of ACF crystals. Firstly, ACF crystal regeneration experiments were conducted in acetone (ACT) and methyl acetate (MA), and it was found that the broken crystals could be successfully regenerated and restored to their original morphology, the regenerated ACF crystals in MA exhibited a larger aspect ratio. Secondly, the crystals obtained from the two solvents were placed in different solvents for regrowth, and it was shown that solvent was a key factor influencing the aspect ratio of ACF crystals. Additionally, HPMC was used to regulate the crystal morphology, it was found that the best effect was achieved when the mass fraction of HPMC was 0.5%, resulting in a regenerated crystal with an aspect ratio of only 2.19. Molecular simulation results indicated that the interaction between the radial (1 1 0) crystal facet and the solvent was weaker than that with the axial (1 0 -1) crystal facet, leading to a higher radial growth rate and a larger aspect ratio of the crystal. However, after adding HPMC, the interaction between HPMC and the radial (1 1 -1) and (1 1 0) crystal facets became stronger. HPMC selectively adsorbed on these two crystal facets, ultimately resulting in crystals with a smaller aspect ratio. The research findings of this study will provide theoretical basis for solving the problem of difficult morphology control due to crystal fragmentation in the pharmaceutical industry production process.

Key words: Crystal growth; Crystal morphology; HPMC; Crystal regeneration mechanism

1. Introduction

Crystallization is a fundamental process in which solute atoms, ions, or molecules gradually come together in a specific arrangement to form crystals under suitable conditions [1]. This process can be divided into two stages: nucleation and growth [2]. Nucleation is the initial stage in which a nucleus is formed in the solution. Crystal growth commences with the deposition of solute on the surface of the nucleus, leading to the gradual expansion and formation of crystals. Once crystal growth ceases, the size and shape of the crystal become fixed. Numerous factors, including temperature [3], solvent [4], solution saturation [5], additives [6], and pH [7] , influence this process. Each crystal material has its own unique growth mechanisms and morphologies, necessitating the selection of appropriate growth methods for each material. Crystal growth finds wide applications in scientific research, material synthesis, and fabrication of electronic devices. For instance, it is utilized in the production of semiconductor materials [8], optical devices [9], and biological crystals. Scientists continuously research and improve crystal growth techniques to enhance crystal quality and properties.

Crystal defects [10], including point defects and dislocations, can occur during the process of crystal growth. Under certain conditions, these defects can partially repair themselves by rearranging and moving [11]. Some self-repairing ceramic materials [12] and polymer crystal materials [13] have demonstrated this self-repairing behavior. Furthermore, certain crystalline materials can undergo plastic and elastic deformation, as well as recrystallization, when subjected to slight external stresses. These materials possess intrinsic properties that enable them to self-repair [14]. The phenomenon of self-healing in crystals has been extensively studied by scientists. However, the reasons behind growth cessation or the formation of multiple crystals resulting from crystal breakage in industrial settings remain unclear. Therefore, this study aims to investigate the regeneration of ACF crystals by intentionally fracturing or partially breaking them, and subsequently introducing solutions or substances externally to restore their integrity and continuity under supersaturation.

However, to artificially fragment a crystal, it is necessary to first determine the location from which the crystal will be cut. This requires identifying the cleavage plane, which is a plane within the crystal that has a distinct structural strength difference due to a specific arrangement of atoms or ions [15]. Cleavage plane in crystals were often composed of planes with weak bond strengths between atoms, molecules, or ions. The crystal's susceptibility to fracture or exfoliation along a disintegration plane is due to the lower binding energy on that plane, resulting in smaller fracture energy [16]. In this study, the crystal morphology of ACF using the attachment energy module and determined the cleavage plane corresponding to the ACF crystal to be the (1 0 -1) facet, Fig 1(a) illustrates the cleavage performed on the ACF crystal, while Figs 1(b) and 1(c) show the actual cleavage of the crystal.

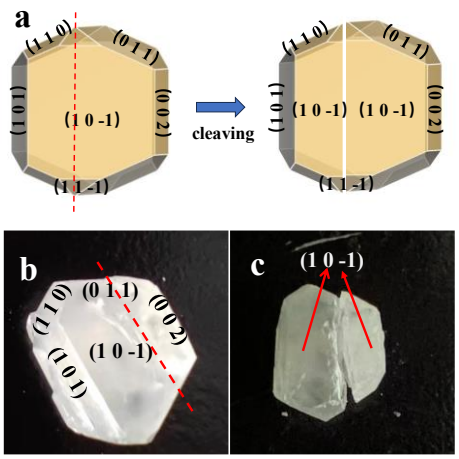

Fig. 1 (a) ACF crystal habit obtained by simulation, (b) and (c) morphology of actual and broken crystals

2. Experiment

2.1 Materials

ACF ($C_{16}H_{13}C_{l2}NO_4$, CAS No. 89796-99-6, 98.0%) was purchased from Shanghai Aladdin Biochemical Technology Co. Hydroxypropyl methyl cellulose polymer (HPMC, viscosity 50mPa.s) was purchased from Shanghai McLean Biochemical Co. ACT (C_3H_6O, CAS No. 67-64-1, 99.5%) and MA ($C_3H_6O_2$, CAS No. 79-20-9, 98.0%) were purchased from Xilong Science Co. All reagents were of analytical grade and were used without further purification. The molecular structures

of ACF and HPMC are shown in Fig 2.

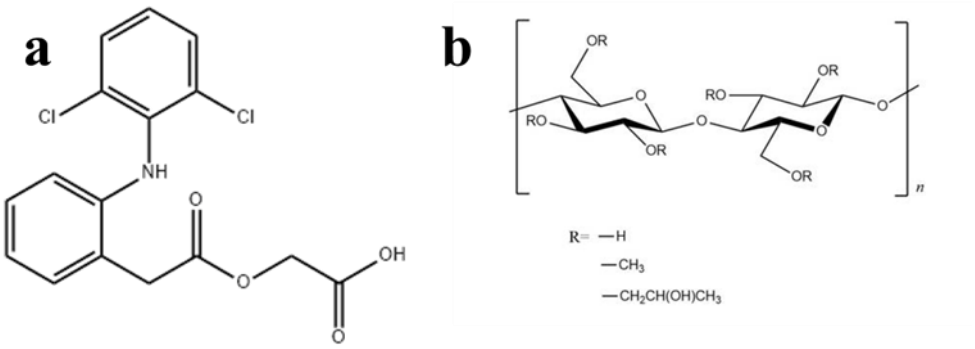

Fig. 2 (a) shows the structural formula of ACF and (b) shows the structural formula of HPMC.

2.2 Preparation of Crystal Seeds

A 20 ml glass screw-top vial containing a specific amount of ACT (MA) was stirred with an excess of ACF at 50 °C for 10 minutes using a DF-101S collector-type thermostatic magnetic stirrer until the ACF completely dissolved. The stirring was then stopped, and the magnet was removed. The solution was allowed to naturally cool to achieve a supersaturated state at 30 °C. To prepare the seed crystals, the solution was cooled down to room temperature naturally, the cap was unscrewed and the bottle's mouth was sealed with a plastic wrap that was punctured 1-3 times to allow the solvent to slowly evaporate at a steady pace at room temperature. The evaporation proceeded for a week. Once the crystals grew to a size of 3-5 mm, they were carefully removed using tweezers and dried.

2.3 Crystal Cutting

The crystals were cut using a scalpel, following the cutting method depicted in Fig. 1. The study examined the regrowth of crystals after cutting in three different orientations (i.e. transverse (T), longitudinal (L), and diagonal (D)). In the transverse (T) cut, pressure was applied to the (1 0 -1) side of the crystal, causing it to break in the middle. For the longitudinal (L) and diagonal (D) cuts, pressure was exerted on the (1 0 -1) facet along the longitudinal (L) and diagonal (D) directions, respectively, to bisect the crystal.

2.4 Crystal Regrowth

Based on Equation (1) and the solubility data of ACF at 30 °C, a supersaturated

solution (S = 1.2) was prepared.

$$S = C_0/C \qquad (1)$$

where C_0 is the actual concentration of ACF and C is the solubility of ACF at 30°C. The small crystals resulting from the cutting were tied with Kevlar fibers and placed in 20 ml glass screw-top bottles containing ACF supersaturated solution (S = 1.2). The bottle openings were covered with plastic wrap to prevent concentration changes in the solution caused by solvent evaporation. The crystal growth process was observed and recorded using a 1600-fold magnification Ray Ban USB microscope from various angles on both sides of the small crystals (Fig 3). Photographs were taken at 1-hour intervals against a black background.

HPMC was used to regulate the aspect ratio of ACF crystals in MA. HPMC solution was applied to the fractured facet of the crystals or different mass fractions of HPMC were added to the ACF supersaturated solution (S = 1.2) to investigate the effect of HPMC on the morphology of ACF crystals.

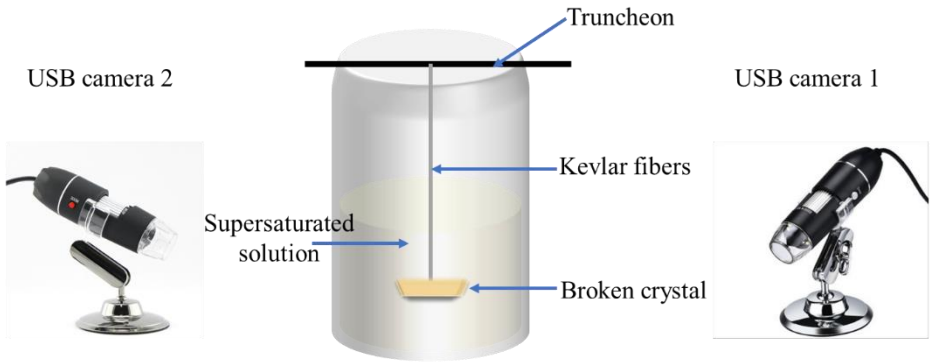

Fig. 3 Experimental set-up to study crystal regeneration.

2.5 Measurement of Growth Rate

The length of the crystals captured by the USB microscope was measured using an inverted microscope equipped with a CCD digital camera with 3.1 million pixels (CNOPTEC BK6000 laboratory microscope). The growth rate of the crystals throughout the regeneration process was then calculated using Equation (2).

$$G = \frac{dL}{dt} \qquad (2)$$

where G represents the growth rate of the crystal, L represents the feature length,

and t represents the time.

2.6 Simulation Process

The simulations were conducted using Material Studio 2020. The crystal structure of ACF was obtained from the Cambridge Crystal Database Center (reference number: 1936959). ACF belongs to the P21/n(14) space group with dimensions of a = 12.1441 Å, b = 8.2073 Å, c = 15.3263 Å, and angles of α = 90°, β = 95.053°, and γ = 90° [17]. Prior to simulating the crystals, the cell was optimized using the COMPASS II force field in the Forcite module. The optimized results were consistent with the cell parameters of ACF in the literature.

Two systems were established: an additive-crystal system consisting of HPMC and ACF crystal layers, and a solvent-crystal system comprising a solvent layer and a crystal layer [18]. In the additive-crystal system, the crystal's morphology was predicted using the attachment energy model in the Morphology Tool module. The principal crystal facets of the resulting crystal habit were divided into three layers and expanded into a supercell larger than 31 Å using the Supercell module. A vacuum layer of 50 Å was applied above it to eliminate boundary effects. The polymer box, pre-built using the Amorphous Cell built polymer boxes, was inserted between the crystal layer and the vacuum layer to form a layer consisting of crystals and polymers [19]. The geometry optimization and dynamics simulation of the constructed layer were performed using the Forcite module under the COMPASS II force field. The dynamics optimization was conducted with the NVT system at 303 K. The total simulation time was set to 100 ps, with a time step of 1 fs and a total of 100,000 steps. An output frame was generated every 500 steps. For the solvent-crystal system, the HPMC layer was not included, and the remaining steps were consistent with those for the additive-crystal system.

To examine the influence of the polymer additive HPMC on the crystal regeneration process, the interaction energy between the polymer and the crystal facet was calculated using Equation (3) [20]. After completing the kinetic optimization of the solvent-crystal system, the mean square displacement (MSD) and radial distribution function (RDF) between the solvent and crystal were computed.

$$E_{int} = E_{tot} - E_{crystal} - E_{polymer} \qquad (3)$$

where E_{int} is the interaction energy between HPMC and the crystal facet, E_{tot} is the total energy of the system, $E_{crystal}$ is the energy of the crystal layer, and $E_{polymer}$ is the energy of the polymer.

3. Results and discussion

3.1 Crystal Regeneration in ACT and MA

Experimental results showed that all the broken ACF crystals were successfully recovered in both ACT and MA solvents. Moreover, the regenerated crystals showed some growth compared to the initial broken crystals. Based on Figs. 4 and 5, the crystals regenerated in MA exhibited longer prismatic crystals, with a larger aspect ratio than those regenerated in ACT. Further observation of the regeneration process in both solvents revealed that the crystals consistently grew towards the broken face first and preferentially returned to their original shape. During this process, the growth rate of the other faces was notably slower. Once the crystals were restored to their original shape, growth continued. This experiment was repeated, yielding consistent results.

Based on the two sets of experimental phenomena, we propose a regeneration mechanism for ACF crystals. Regardless of the direction in which ACF crystals are cut, during the initial stage of crystal regeneration, which is the regrowth stage, the crystals tend to grow preferentially towards the broken face to restore the original shape of the crystal. Subsequently, they continue to grow into larger crystals based on this, as shown in Fig 6. To verify this hypothesis, a series of experiments were conducted.

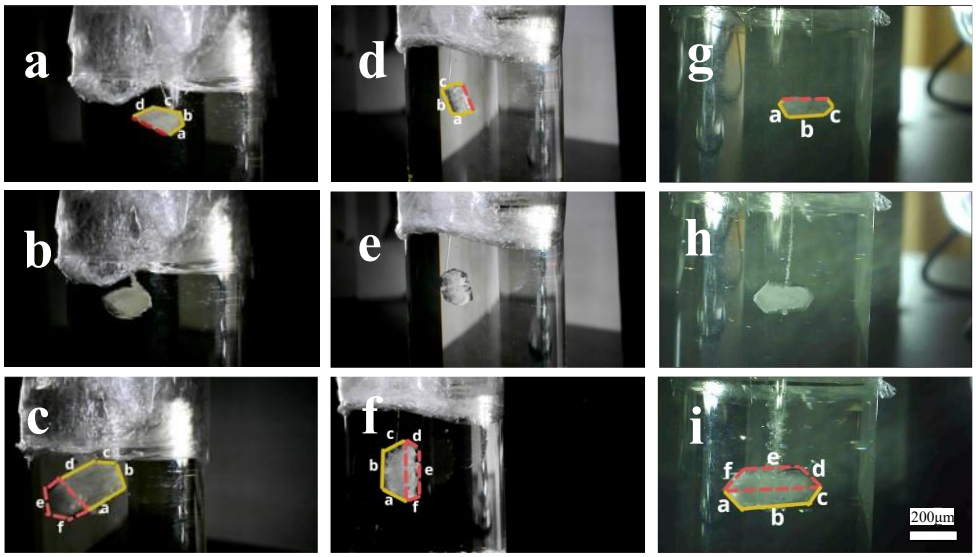

Fig. 4 Regeneration of ACF crystals in ACT (a, b, c are transverse cuts, d, e, f are longitudinal cuts, g, h, i are diagonal cuts)

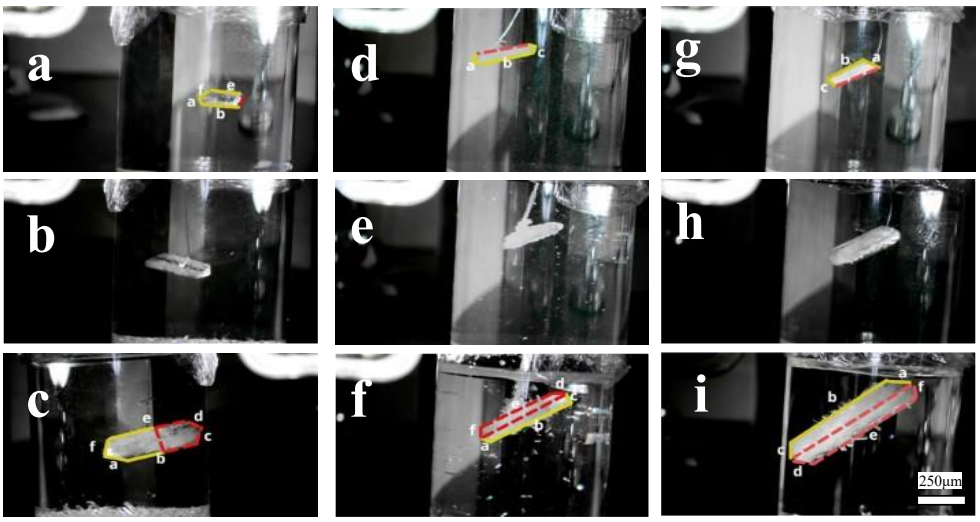

Fig. 5 Regeneration of ACF crystals in MA (a, b, c are transverse cuts, d, e, f are longitudinal cuts, g, h, i are diagonal cuts)

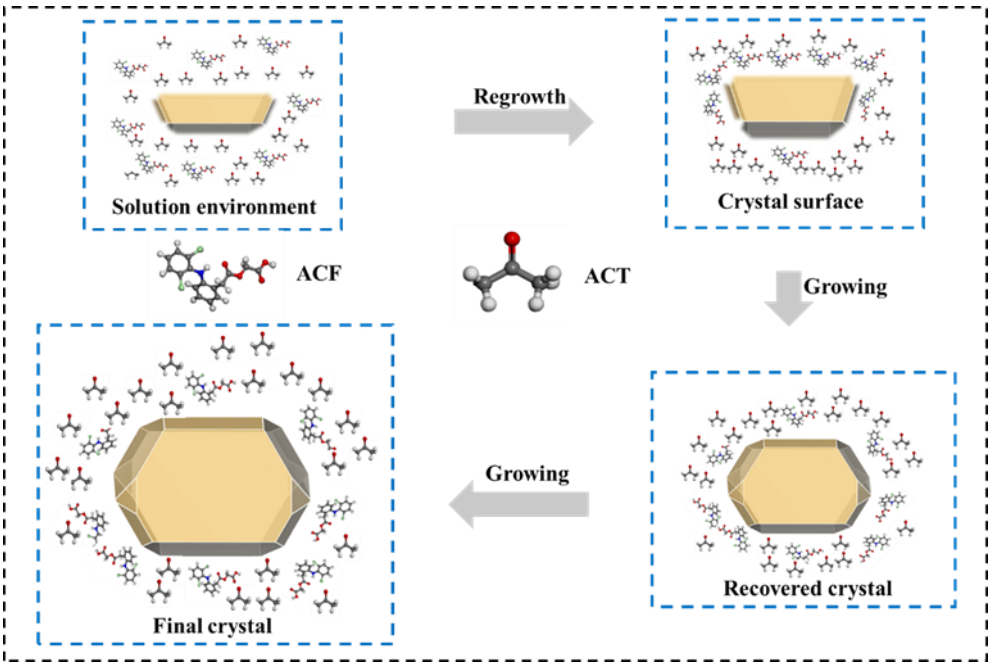

Fig. 6 Regeneration mechanism of ACF crystals

3.2 Solvent's Effect on ACF Crystal Aspect Ratio

In response to the interesting phenomenon observed in Figs 4 and 5, where the aspect ratio of regenerated ACF crystals in MA is significantly larger than that in ACT, crossover experiments were conducted to investigate whether the phenomenon was caused by the intrinsic properties of the crystals themselves or by the effects of the solvent. ACF crystals obtained from incubation in ACT were cut and fragmented, and then regrown in MA. Similarly, ACF crystals obtained from incubation in MA were cut and fragmented, and then regrown in ACT. Both crossover experiments took into account three different cutting orientations (transverse, longitudinal, and diagonal) and their impact on crystal recovery and regrowth. The results of these experiments are presented in Figures 7 and 8.

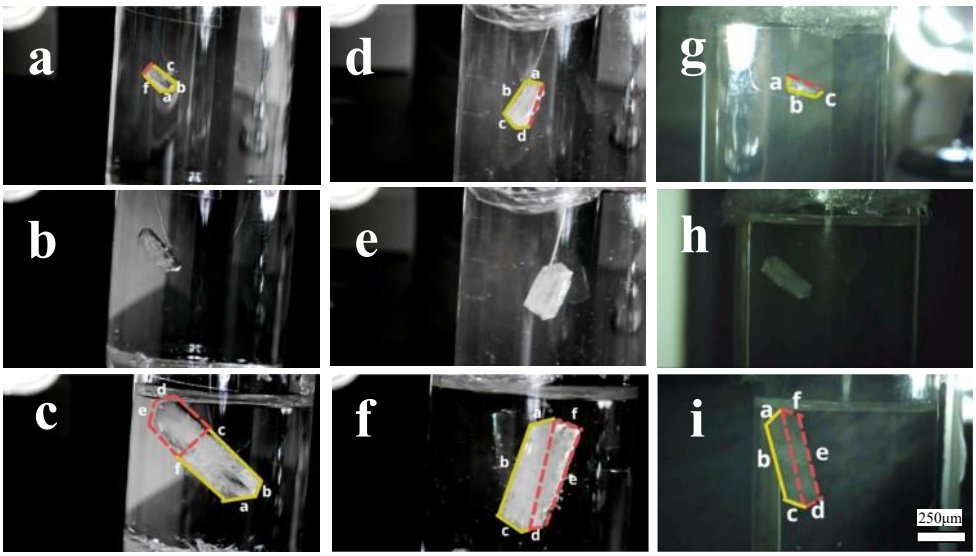

Fig. 7 Regeneration of ACF crystals cultured in ACT in MA (a, b, c are transverse cuts, d, e, f are longitudinal cuts, g, h, i are diagonal cuts)

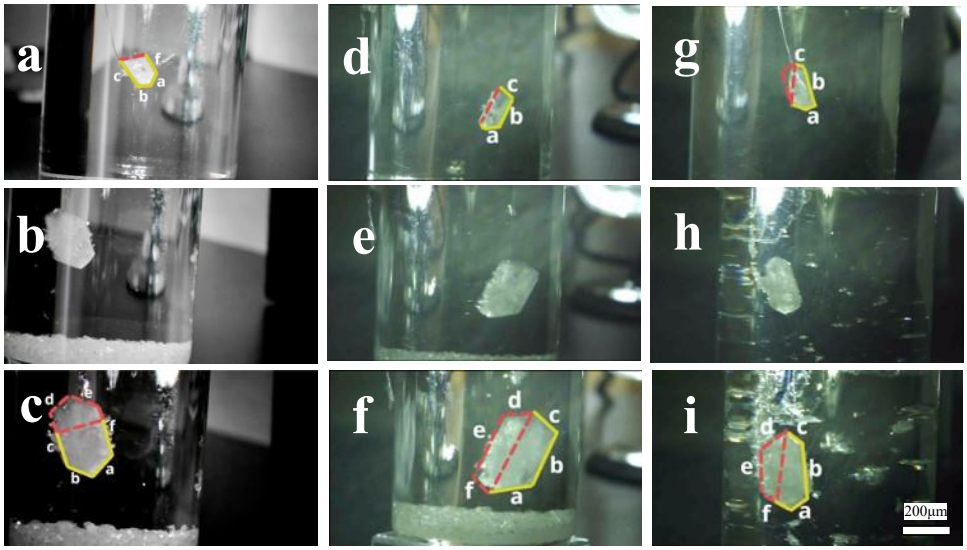

Fig. 8 ACF crystals cultured in MA are regenerated in ACT (a, b, c are transverse, d, e, f are longitudinal, g, h, i are diagonal)

Figs 7 and 8 show that ACF crystals grown in ACT had a larger aspect ratio when fragmented and suspended in MA for regrowth. Conversely, ACF crystals grown in MA had a smaller aspect ratio when suspended in ACT for regrowth compared to their aspect ratio during regrowth in MA. Moreover, Figs. 7 and 8 served as the evidence that supported the growth mechanism proposed in Fig. 6.

To provide further clarity on the disparity in aspect ratios observed in Figs 4, 5, 7, and 8, the characteristic length of each crystal was measured to calculate the aspect

ratios. The results are depicted in Fig 9. From Fig 9(a), the aspect ratio of ACF crystals in MA was approximately twice that of ACF crystals in ACT, indicating a significant difference in aspect ratios between the two solvents. A similar trend is observed in Fig 9(b). Specifically, the aspect ratio of ACF crystals cultured in ACT and regenerated in MA after fragmentation was notably larger than that of the final crystals regenerated in ACT from ACF crystals cultured in MA. These experimental data consistently demonstrated that the aspect ratio of broken ACF crystals regenerated in MA was greater than those regenerated in ACT, irrespective of the solvent used for culturing, suggesting that the solvent employed plays a significant role in the regeneration process.

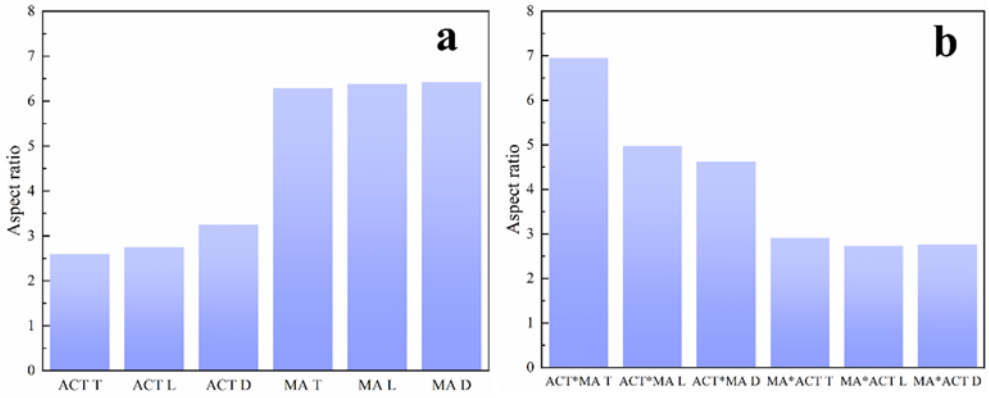

Fig. 9 (a) Aspect ratio of crystals in ACT and MA, (b) Aspect ratio in crossover experiments

3.3 Impact of the Polymer Additive HPMC on the Recovery and Regeneration of ACF Crystals

The concept of crystal habit refers to the unique features displayed by crystals during their formation and growth. These features ultimately determine the structure, properties, and potential applications of the crystals [21]. In industrial settings, crystals with high aspect ratios are generally not desirable as they are vulnerable to fracture and deformation during manufacturing processes. This can adversely affect operations such as filtration and tableting [22, 23]. Consequently, stringent production requirements and precise control of all parameters are necessary, impeding the growth of large-scale crystals. To regulate the aspect ratio of ACF crystals in MA, HPMC as introduced as an additive. HPMC offers several advantages as a regulator of crystal growth rate: it can influence the growth rate by adjusting the energy of the crystal facet [20]. Additionally,

it can interact with the crystal facet to form a complex molecular layer [24]. These molecular layers can be intricate and may adsorb onto the crystal facet during growth [25], thereby influencing the crystal's structure and morphology. Even minute quantities of additives can exert significant effects on the crystal growth process [26]. For these reasons, HPMC was selected to modulate the crystal's structure and morphology to fulfill various requirements.

Two methods were devised to reduce the aspect ratio of the crystals with HPMC: (1) applying the HPMC solution to the broken facet of the crystals, and (2) adding a certain amount of HPMC to the MA solution. It was found that the inhibitory effect of applying the HPMC directly to the broken facet of the crystals was influenced by the facet (Fig 10). After cutting one end of the crystal and coating it with HPMC, the growth of the coated end was significantly inhibited, while the growth rate of the other end was unaffected and continued to grow rapidly. Consequently, the aspect ratio of the crystal did not improve. Longitudinal cutting and HPMC application had no significant effect on the restored growth of the crystal, which grew again to a large aspect ratio. To achieve crystals with smaller aspect ratios, both ends of the ACF crystals were cut transverse and the HPMC solution was applied to both ends for recovery. Contrary to expectations, the experiment did not yield crystals with inhibited growth and a smaller aspect ratio due to the application of HPMC on both ends of the crystal. Instead, many small crystals appeared on the side of the crystal due to secondary nucleation. Finally, when the broken crystals were completely submerged, the crystals did not return to their original morphology but showed disordered growth.

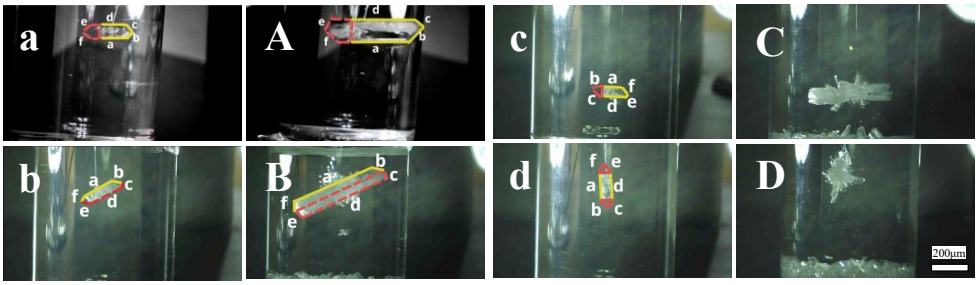

Fig. 10 Crystal regeneration with HPMC applied on the fractured facet; (a-d) and (A-D) represent the application of HPMC to one end of ACF, longitudinal cutting and HPMC application, full immersion of cross-cut ends in HPMC, and the morphology of the crystal before and after HPMC

application to both ends, respectively.

Since the experimental results showed that HPMC inhibited crystal growth, the second method was tested to reduce the aspect ratio of ACF crystals. In the experiment, different concentrations of HPMC were added to the supersaturated ACF solution (i.e. 0.25%, 0.50%, 0.75%, 1.0%, 1.25%, and 1.5% of the mass of ACF; S = 1.2). The results of these experiments are presented in Fig 11. By comparing the regenerated ACF crystals from these experiments with those shown in Fig 5 (MA), it is evident that the direct addition of HPMC to the solution successfully reduced the aspect ratio of the regenerated ACF crystals. Furthermore, the regeneration of ACF crystals was successful in all six sets of experiments.

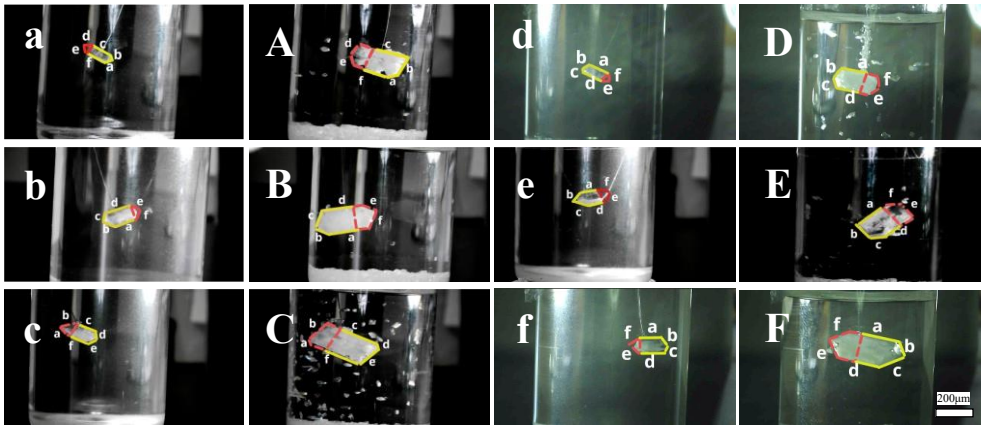

Fig. 11 a-f and A-F show the morphology before and after regeneration of ACF broken by adding 0.25%, 0.50%, 0.75%, 1.0%, 1.25%, 1.5% HPMC, respectively.

Fig 12 illustrates that applying HPMC as a coating on ACF crystals did not lead to an improvement in aspect ratio in the MA. On the contrary, experimental results consistently show that adding HPMC to the solution yields better improvement in the aspect ratio of ACF crystals compared to applying HPMC, regardless of the amount added. The crystal aspect ratio fluctuated with the addition of HPMC. Specifically, when the HPMC addition was 0.25%, the crystal aspect ratio was 2.73. However, the best effect on aspect ratio improvement was observed at an HPMC addition of 0.5%. After improvement, the crystal aspect ratio decreased to only 2.19, with the crystals exhibiting a regular block morphology.

As the mass fraction of HPMC increased from 0.5% to 1.5%, the aspect ratio of

the crystals also gradually increased from 2.19 to 3.18. This suggested a correlation between the addition of HPMC and the increase in aspect ratio of the crystals. When the mass fraction of HPMC was only 0.25%, the crystal facet could not adsorb enough HPMC to effectively inhibit crystal growth. Excessive polymer addition could lead to agglomeration, hindering dispersion in the solution and reducing the inhibition effect on crystal aspect ratio [27].

Overall, the experimental results indicated that the addition of HPMC could improve the aspect ratio of the crystals compared to the final crystals of ACF obtained through recovery and regeneration in the MA. However, it was crucial to strictly control the amount of HPMC added. The best improvement in aspect ratio was achieved when the HPMC concentration was 0.5%, resulting in an aspect ratio of only 2.19.

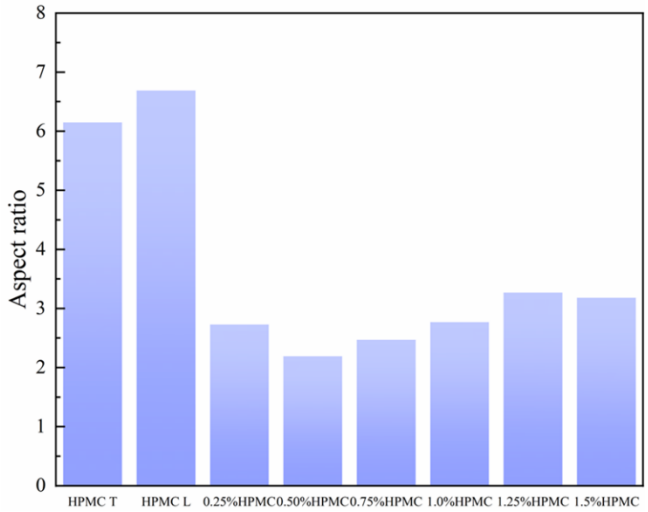

Fig. 12 Improved ACF crystal aspect ratio with HPMC coating and different HPMC concentrations

3.4 Growth Rate of Crystals

In order to better understand the process of crystal regeneration, the growth rates of crystal recovery and regeneration under different solvents, crossover experiments, HPMC coating, and different HPMC concentrations are shown in Figs 13 and 14.

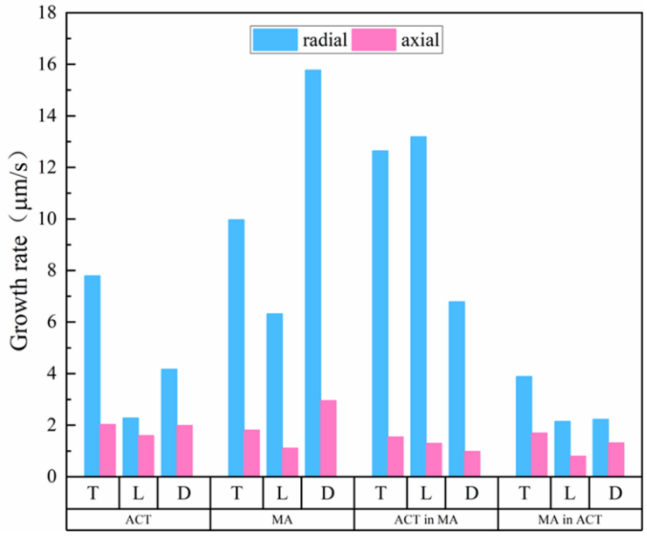

Fig. 13 Crystal recovery growth rates in ACT, MA, and crossover experiments

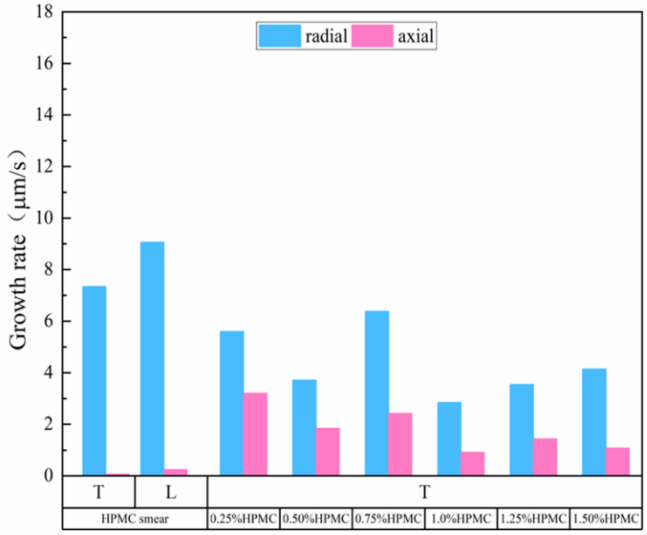

Fig. 14 Crystal recovery growth rate in the presence of HPMC

According to the data presented in Fig 13, the growth rate of ACF crystals was consistently greater in the radial direction than in the axial direction during the regeneration in MA, resulting in ACF crystals with a large aspect ratio. When HPMC was applied as a coating to both the transversely cut end and the longitudinally cut end of the crystals, there was limited growth in the axial direction of the coated ends (Fig 14). Although the application of HPMC reduced the growth rate in the longitudinal direction, it did not improve the aspect ratio of the crystals due to the slower growth rate in the axial direction.

Comparing the growth rates of ACF crystals regenerated in MA (shown in Fig 13) to those affected by the addition of HPMC, it was evident that the growth rate in

the radial direction was significantly more suppressed compared to the growth rate in the axial direction. Interestingly, at 1.0% HPMC incorporation, the growth rate of the crystals was lower than at 0.5%, while the aspect ratio of the crystals at 0.5% HPMC (2.19) was lower than at 1.0% (2.77). This discrepancy could be attributed to the fact that although the overall growth rate of the crystals was lower at 1.0% HPMC, the ratio of the radial and axial growth rates was higher at 1.0% (2.77) than at 0.5% (2.02). Consequently, the radial growth rate was much faster than the axial growth rate, resulting in regenerated crystals with a larger aspect ratio compared to those at 0.5%.

In summary, the longitudinal direction of the crystals had preferential growth over the axial direction. When growth was inhibited at one end of the radial direction, the crystals could continue to grow toward the other end with insignificant changes in the aspect ratio. When both ends were suppressed, the desired rapid growth in the axial direction did not occur, and the cut crystal did not recover its habit with secondary nucleation occurring in the axial direction on the crystal facet.

3.5 Reasons for the Difference in Crystal Aspect Ratio in the Two Solvents

3.5.1 Mean Square Displacement (MSD)

Since the morphology of a crystal can be significantly affected by the interaction between the solvent and the crystal facet, it is important to consider the role of the solvent [28]. The diffusion coefficient (D) of ACF in both solvents was calculated using Material Studio 2020 software. D also represents the solvent's ability to diffuse at the crystal facet (i.e. the probability of a particle moving from one position to another by free diffusion per unit of time). D is mathematically defined as the derivative of the mean square displacement (MSD) with respect to time in Equation (4) [29], where MSD is the average of the squares of the changes in particle position during a given time interval [30]. The r_i value was calculated using the analytical method of MSD in the Forcite module after applying the geometric and kinetic optimizations mentioned in the simulation section above. The data from 10-100 ps, which showed a relatively smooth curve, was selected. D was calculated by summing the r_i values using Eq. (4) [31]. The

results are listed in Table 1.

$$D = \frac{1}{6}\lim_{t\to\infty}\frac{d}{dt}\sum_{i=1}^{N}\langle|r_i(t) - r_i(0)|^2\rangle (4)$$

where t represents the time, r_i represents the position of the solvent molecule at time i, N is the number of molecules.

Table 1 Diffusion coefficients of ACF at each crystal facets in ACT and MA.

Facet	D（$10^{-9}m^2/s$）	D（$10^{-9}m^2/s$）
	ACT	MA
(1 0 -1)	4.8223	6.5011
(1 0 1)	4.6572	5.8784
(0 0 2)	4.2319	5.0414
(0 1 1)	3.3346	1.7023
(1 1 0)	4.0644	4.3232
(1 1 -1)	3.6281	1.6027

Large D means a strong the interaction between the solvent and the crystalline facet, and the solvent tends to adsorb onto it [29, 32]. When the solvent readily adsorbs onto the crystalline facet, it is more difficult for the solute to absorb onto the crystalline facet, resulting in a slower growth rate of the crystalline facet, and a higher surface occupancy of the crystalline facet at the end.

Table 1 shows the following order of D values: in ACT (1 0 -1) > (1 0 1) > (0 0 2) > (1 1 0) > (1 1 -1) > (0 1 1); in MA, (1 0 -1) > (1 0 1) > (0 0 2) > (1 1 0) > (0 1 1) > (1 1 - 1). In both ACT and MA, the D value of the (1 0 -1) face is larger than that of the (1 1 0) face, which makes the growth rate of the (1 1 0) face larger than that of the (1 0 -1) face, and ultimately leads to the (1 0 -1) face being the main crystal facet, and the faster growth rate of the (1 1 0) face makes the whole crystal elongate in the radial direction, leading to a larger aspect ratio. This is also consistent with the experimental data that regardless of the solvent, the crystals always exhibited high aspect ratios as long as the regeneration was resumed in MA after fragmentation.

3.5.2 Radial Distribution Function (RDF)

In addition to MSD, radial distribution function (RDF) was used to analyze

specific atoms. RDF represents the probability of a selected particle appearing near other atoms at a given distance [33]. The RDF curves of (1 0 -1) and (1 1 0) crystal facets were investigated to explore the effect of the solvent on the crystal morphology. Based on the value of r corresponding to the RDF curves, the interactions were categorized into three types, i.e., hydrogen bonding with r less than 3.1 Å, van der Waals interactions with r between 3.1 and 5.0 Å, and electrostatic interactions with r greater than 5.0 Å [34]. Figure 15 shows the RDF plots of (1 0 -1) and (1 1 0) in the two solvents.

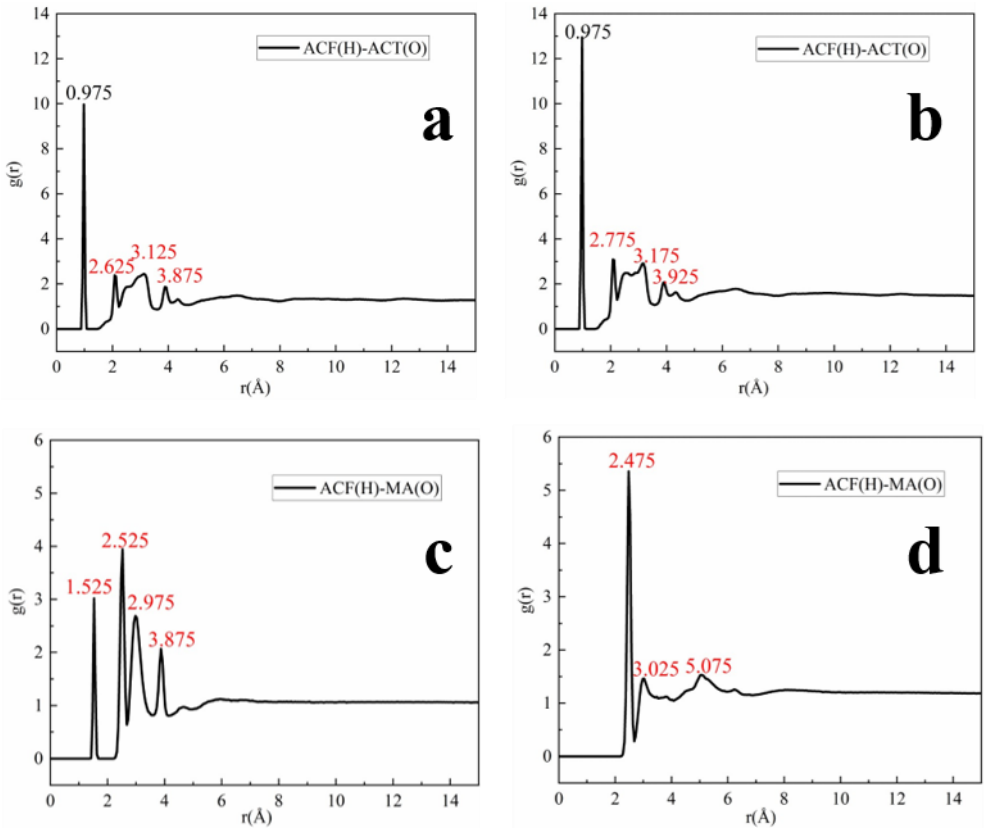

Fig. 15 (a) (b) (1 0 -1), (1 1 0) face RDF curves in ACT, (c) (d) (1 0 -1), (1 1 0) face RDF curves in MA

Fig 15 shows that the r values for most of the RDF curves for the (1 0 -1) and (1 1 0) facets in both solvents are less than 3.1 Å, indicating that the interactions between the (1 0 -1) and (1 1 0) facets and the solvents in both ACT and MA are primarily due to hydrogen bonding. Comparing Figs. 15a, b, c, and d, it is evident that the r value for curve b (2.775) is greater than that for curve a (2.625). This trend is also observed in curves c and d, where the r values (2.475, 3.025) are greater than those in curve c (1.525, 2.525, 2.975). These results indicate that the interaction of the (1 1 0) face with ACT or

MA is weaker than that of the (1 0 -1) face with ACT or MA in both ACT and MA [35, 36].

The stronger interaction of the (1 0 -1) facet with ACT or MA in the axial direction leads to a higher likelihood of solvent adsorption on this surface. Consequently, the corresponding solute will find it more difficult to adsorb onto the (1 0 -1) facet, resulting in a slower growth rate in the axial direction. On the other hand, the (1 1 0) facet, which is positioned in the longitudinal direction, exhibits a weaker interaction with the solvent. This makes it more favorable for the solute to adsorb onto the (1 1 0) facet, leading to growth along the (1 1 0) direction. The crystals had elongated prismatic shapes in both solvents due to the faster growth rate in the longitudinal direction.

In addition, it can be seen that the r-value of part c (1.525, 2.975) is larger than the r-value of part a (0.975, 2.625), and the r-value of part d (2.475, 3.025) is larger than that of part b (0.975, 2.775). These results highlight that the r-values vary even for the same crystal facet when different solvents are used. Moreover, in MA, the interaction of the (1 0 -1) and (1 1 0) faces with the solvent is smaller than the interaction of ACT with the (1 0 -1) and (1 1 0) faces. The (1 0 -1) and (1 1 0) faces have stronger interactions with ACT, so ACF molecules are more likely to adsorb on these faces in MA than on ACT. This explains why ACF crystals grow faster in MA than in ACT, ultimately leading to a larger aspect ratio of ACF in MA than in ACT.

3.6 Improvement of ACF Crystal Aspect Ratio in MA by HPMC

The additives interact with the crystal facets, promoting or inhibiting the adsorption of solute molecules. This affects the growth rate and ultimately changes the crystal morphology. Fig 16 illustrates the interaction process between HPMC and (1 0 -1) crystal facets from the first to the twentieth frame. It is evident that the (1 0 -1) facets are primarily exposed to carbon-based and hydroxyl groups, which can create hydrogen bonds with HPMC. A previous study found that HPMC gradually adsorbed onto the crystal facets of ACF, affecting their growth [6].

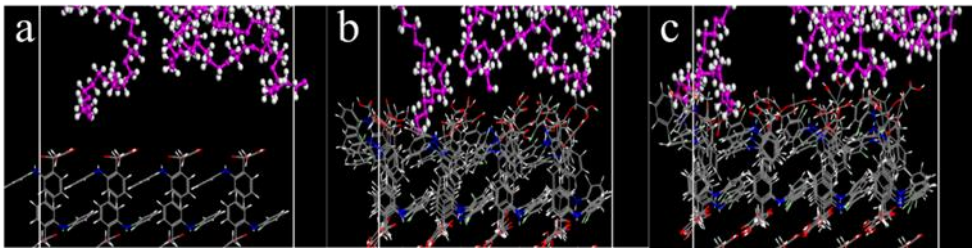

Fig. 16 Interaction of HPMC and (1 0 -1) crystal facet, (a) first frame (b) 10th frame (c) 20th frame

According to Equation (3), the interaction energy E_{int} between HPMC and the crystal facet was calculated using molecular dynamics simulation, and the results showed that the values were negative, indicating that HPMC has an adsorption effect on the crystal facets of ACF. To facilitate comparison and analysis, the obtained interaction energies are presented in absolute values in Fig 17.

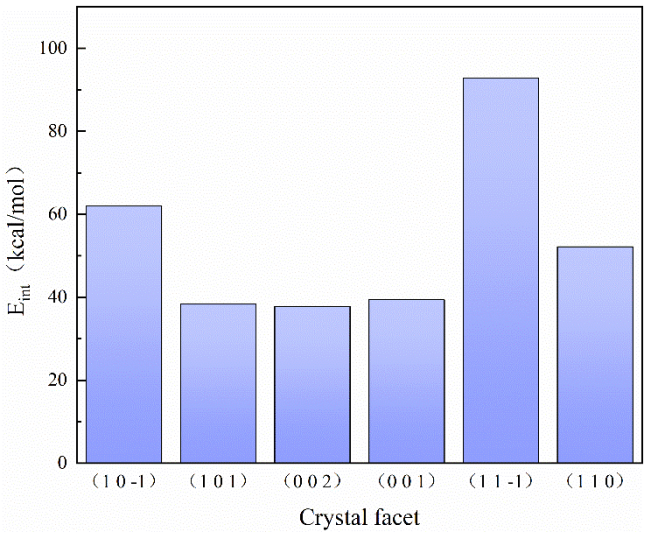

Fig. 17 Interaction energy of HPMC and crystal facets

The interaction energies of HPMC and ACF crystal facets follow the order of (1 1 -1) > (1 0 -1) > (1 1 0) > (0 1 1) > (1 0 1) > (0 0 2). The longitudinal faces (1 1 -1) and (1 1 0) have interaction energies of 92.92 kcal/mol and 52.26 kcal/mol, respectively, while the axial face (1 0 -1) has an interaction energy of 62.10 kcal/mol.

As observed, the interaction with HPMC in the longitudinal direction is stronger than that in the axial direction, resulting in a greater inhibition effect of HPMC on the longitudinal direction than the axial direction [20]. HPMC is more likely to adsorb in the longitudinal direction, ultimately leading to the formation of crystals with a smaller

aspect ratio [31].

3.7 Mechanism of HPMC-regulated Crystal Morphology

The mechanism of HPMC-regulated recovery and regeneration of ACF crystals is proposed based on the experimental results and molecular dynamics simulations (Fig 18).

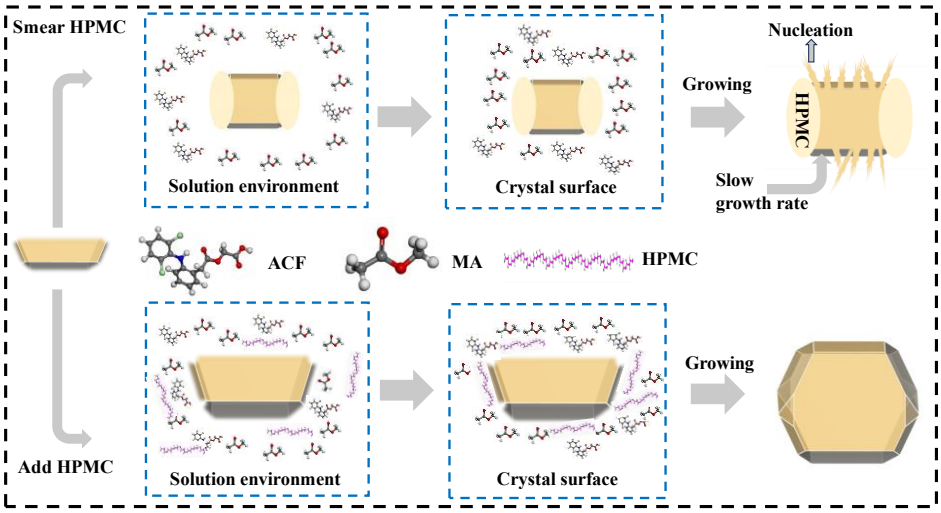

Fig. 18 Mechanism of HPMC-regulated regeneration of ACF crystals.

The upper path in Fig 18 illustrates the crystal growth mechanism when HPMC is applied to the broken faces of the crystals. The growth of crystals with HPMC applied at both ends is used as an example. The MSD and RDF analysis reveals that solute molecules preferentially adsorb on the (1 1 0) face in the radial direction over the (1 0 -1) face in the axial direction., leading to rapid crystal growth in the radial direction and slow growth in the axial direction. Applying HPMC to the ends of the radial direction inhibits radial growth and slows axial growth, preventing the desired rapid axial growth and resulting in secondary nucleation on the sides of the crystal (i.e. the formation of many small crystals). As a result, the crystal did not return to its original form. The lower path in Fig 18 illustrates the growth mode of ACF crystals in the presence of dissolved HPMC, where the molecules of ACF, MA and HPMC are arranged in a disordered manner in a solution environment. On the crystal facet, HPMC tends to be adsorbed in the longitudinal direction due to the stronger interaction with the longitudinal (1 1 -1) than the axial (1 0 -1), which impedes the adsorption of ACF molecules in the longitudinal direction. Therefore, the aspect ratio of the crystal

decreases.

4. Conclusions

The current study investigates the regeneration process and mechanism of crystals using ACF as the model molecule. Conclusions are based on the data of crystal seed preparation, crystal recovery experiments, polymer regulated growth experiments, and molecular simulation calculations.

The broken ACF crystals could regenerate and grow well in both ACT and MA solvents, with the crystals primarily regrowing along the direction of the fracture to restore their original morphology before further growth occurs. The aspect ratio of the regenerated crystals in MA was always greater than that in ACT, because the interaction between the radial (1 1 0) crystal facet and MA was weaker than that with ACT. Compared to ACT, MA was more likely to diffuse to the axial (1 0 1) crystal facet. Therefore, ACF molecules were more easily adsorbed onto the (1 1 0) crystal facet in MA than in ACT, resulting in a larger aspect ratio of ACF crystals in MA.

HPMC effectively regulated the aspect ratio of ACF. The best regulation was achieved when the mass fraction of HPMC was 0.5%. The radial growth rate decreased from 9.97 μm/s to 3.71 μm/s, and the aspect ratio decreased from 6.29 to 2.19, resulting in the formation of bulk ACF crystals. Molecular simulation shows that HPMC interacts more strongly with crystal facets in the order of (1 1 -1) > (1 0 -1) > (1 1 0) > (0 1 1) > (0 1 1) > (0 0 2). This makes HPMC more likely to be adsorbed on the radial (1 1 -1) and (1 1 0) crystal facets, resulting in the suppression of the crystal's aspect ratio.

Declaration of interest

The authors declare that they have no known competing financial interests or personal relationships that could have appeared to influence the work reported in this paper.

Acknowledgments

This work was financially supported by National Natural Science Foundation of China (grant No. 22068002 and 22178054), Jiangxi Provincial Natural Science Foundation (grant No. 20224ACB213007, 20212ACB203002, and 20232BBH80015),

Jiangxi Province Key Laboratory of Synthetic Chemistry (grant No. JXSC202209).

References:

[1]. K., V.K., et al., Nonclassical crystal growth and growth rate hysteresis observed during the growth of curcumin in impure solutions. CrystEngComm, 2023.

[2]. Soto, R. and Å.C. Rasmuson, Crystal Growth Kinetics of Piracetam Polymorphs in Ethanol and Isopropanol. Crystal Growth & Design, 2019.

[3]. Plummer, L.K., et al., Influence of Monomer Flux and Temperature on Morphology of Indium Oxide Nanocrystals during a Continuous Growth Synthesis. Chemistry of Materials, 2019.

[4]. Chai, Y., et al., Investigating the Solvent Effect on Crystal Nucleation of Etoricoxib. Crystal Growth & Design, 2019.

[5]. Isaac, A.L., et al., Crystal Nucleation and Growth: Supersaturation and Crystal Resilience Determine Stickability. Crystal Growth & Design, 2023.

[6]. Shuai, Y., et al., Effect of natural polymer additives on crystal form and morphology of clozapine anhydrate and monohydrate. Journal of Molecular Liquids, 2022.

[7]. Chen, W.C., et al., The influence of pH on the habit and the rate of α-LiIO3 crystal growth. Journal of Crystal Growth, 1987.

[8]. Ding, C., et al., Wafer-scale single crystals: crystal growth mechanisms, fabrication methods, and functional applications. Journal of Materials Chemistry C, 2021.

[9]. Jeon, T., et al., Hybrid Perovskites: Effective Crystal Growth for Optoelectronic Applications. Advanced Energy Materials, 2017.

[10]. Kojima, K., Crystal growth and defect control in organic crystals. Progress in Crystal Growth and Characterization of Materials, 1992.

[11]. Commins, P., H. Hara and P. Naumov, Self‐Healing Molecular Crystals. Angewandte Chemie International Edition, 2016.

[12]. Ozaki, S., T. Osada and W. Nakao, Finite element analysis of the damage and healing behavior of self-healing ceramic materials. International Journal of Solids and Structures, 2016.

[13]. Zhang, L., et al., Hyperexpandable, self-healing macromolecular crystals with integrated polymer networks. Nature, 2018.

[14]. Commins, P., et al., Efficiently self-healing boronic ester crystals. Chemical Science.

[15]. Bade, I., et al., Crystal regeneration – a unique growth phenomenon observed in organic crystals post breakage. Materials Horizons, 2023.

[16]. Vaknin, U., D. Sherman and S. Gorfman, Geometrical prediction of cleavage planes in crystal structures. IUCrJ, 2021.

[17]. Jelsch, C., et al., Aceclofenac and interactions analysis in the crystal and COX protein active site. Journal of Molecular Structure, 2020.

[18]. Yan, W., et al., Insight into the morphology and crystal growth of DL-methionine in aqueous solution with presence of cellulose polymers. Journal of Molecular Liquids, 2021.

[19]. Cui, P., et al., The effect of solvents on crystal morphology of sucralose: experiments and molecular dynamics simulation studies. Journal of Crystal Growth, 2020.

[20]. Ying, H., et al., Effects of polymers on the regulation of p-aminobenzoic acid crystal habit. Journal of Molecular Liquids, 2023.

[21]. Liangcheng, S., et al., Crystal morphology regulation of pronamide through solvent selection: Prediction and implementation. The Journal of Chemical Thermodynamics, 2022.

[22].Li, J. and M.F. Doherty, Steady State Morphologies of Paracetamol Crystal from Different Solvents. Crystal Growth & Design, 2017.

[23]. Shengzhe, J., et al., Process intensification and control strategies in cooling crystallization: Crystal size and morphology optimization of α-PABA. Chemical Engineering Research and Design, 2022.

[24]. Shi, S. and C. Su, Corrosion Inhibition of High Speed Steel by Biopolymer HPMC Derivatives. Materials, 2016.

[25]. Chen, N., et al., Water Retention Mechanism of HPMC in Cement Mortar. Materials, 2020.

[26]. Chavan, R.B., et al., Evaluation of the inhibitory potential of HPMC, PVP and HPC polymers on nucleation and crystal growth†. RSC Advances, 2016.

[27]. Yan, W., et al., Polymer-mediated and ultrasound-assisted crystallization of ropivacaine: Crystal growth and morphology modulation. Ultrasonics Sonochemistry, 2023.

[28]. Marinova, V., et al., Solvent Dynamics and Thermodynamics at the Crystal–Solution Interface of Ibuprofen. Crystal Growth & Design, 2019.

[29]. Qianjin, G. and Z. Shuhai, A theoretical investigation into the effect of solvent on crystal morphology of 1-methyl-3,4,5-trinitro-1H-pyrazole (MTNP). Journal of Crystal Growth, 2022.

[30]. Wallace, D.C., G. De Lorenzi-Venneri and E.D. Chisolm, Atomic motion from the mean square

displacement in a monatomic liquid. Journal of Physics: Condensed Matter, 2016.

[31]. Dongbo, W., et al., Revealing the Effects of Additives with Similar Structures on Crystal Growth: A Case Study of l-Alanine. Crystal Growth & Design, 2023.

[32]. Mingzhe, T., et al., Uncovering the Coupling Mechanism of Enhanced Growth of Acephate by Additives: Experiments and Molecular Dynamics Simulations. Crystal Growth & Design, 2023.

[33]. Zidan, C., et al., Exploring the solvent effect on risperidone (form I) crystal morphology: A combination of molecular dynamics simulation and experimental study. Journal of Molecular Liquids, 2023.

[34]. Zhao, P., et al., Predicting the crystal habit of photoinitiator XBPO and elucidating the solvent effect on crystal faces†. CrystEngComm, 2019.

[35]. Haixia, H., et al., Exploring the solvent effect on crystal morphology of naphazoline hydrochloride: Molecular dynamic simulations and experiments. Journal of Molecular Liquids, 2023.

[36]. Li, L., et al., Effect of the solvent on the morphology of sulfamerazine crystals and its molecular mechanism. CrystEngComm, 2022.